Published in final edited form as:
Neuron. 2008 October 9; 60(1): 56–69. doi:10.1016/j.neuron.2008.09.028.

Tbr2 Directs Conversion of Radial Glia into Basal Precursors and Guides Neuronal Amplification by Indirect Neurogenesis in the Developing Neocortex

Alessandro Sessa[1,4], **Chai-an Mao**[2,4], **Anna-Katerina Hadjantonakis**[3], **William H. Klein**[2], and **Vania Broccoli**[1,*]

[1]Molecular Neuropathology Laboratory, SCRI, San Raffaele Scientific Institute, Via Olgettina 58, 20132 Milan, Italy

[2]Department of Biochemistry and Molecular Biology, The University of Texas M.D. Anderson Cancer Center, Houston, TX 77030, USA

[3]Developmental Biology Program, Sloan-Kettering Institute, New York, NY 10065, USA

Summary

T-brain gene-2 (*Tbr2*) is specifically expressed in the intermediate (basal) progenitor cells (IPCs) of the developing cerebral cortex; however, its function in this biological context has so far been overlooked due to the early lethality of *Tbr2* mutant embryos. Conditional ablation of *Tbr2* in the developing forebrain resulted in the loss of IPCs and their differentiated progeny in mutant cortex. Intriguingly, early loss of IPCs led to a decrease in cortical surface expansion and thickness with a neuronal reduction observed in all cortical layers. These findings suggest that IPC progeny contribute to the correct morphogenesis of each cortical layer. Our observations were confirmed by tracing $Tbr2^+$ IPC cell fate *using Tbr2*::GFP transgenic mice. Finally, we demonstrated that misexpression of *Tbr2* is sufficient to induce IPC identity in ventricular radial glial cells (RGCs). Together, these findings identify Tbr2 as a critical factor for the specification of IPCs during corticogenesis.

Introduction

Little is known about how the cerebral cortex reaches such a level of complexity in humans and exhibits unique cortical field specialization and regional cytoarchitecture along mammalian evolution (Molnár et al., 2006; Krubitzer, 2007; Bystron et al., 2008). However, the cellular and molecular processes promoting the impressive expansion of the neocortical field during both ontogenesis and phylogeny have begun to be delineated (Monuki and Walsh, 2001; Rakic, 2006; Kriegstein et al., 2006). The cerebral cortex emerges from the dorsal neuroepithelium of the telencephalon during embryonic development. Cell proliferation in two distinct mitotically active layers drives cortical expansion. Lining the telencephalic ventricular surface, radially oriented radial glia cells (RGCs) constitute the ventricular zone (VZ) (Kriegstein and Götz, 2003; Rakic, 2000; Götz and Huttner, 2005), while basally located intermediate progenitor cells (IPCs), also known as basal progenitors or non-surface-dividing (NS-div) cells, extend up to the intermediate zone (IZ), where they populate the subventricular layer (SVZ) (Noctor et al., 2004; Haubensak et al., 2004; Miyata et al., 2004). RGCs display

*Correspondence: broccoli.vania@hsr.it.
[4]These authors contributed equally to this work

Supplemental Data
The Supplemental Data can be found with this article online at http://www.neuron.org/supplemental/S0896-6273(08)00807-6.

a defined apico-basal polarity with a specialized apical membrane domain facing the ventricle that is limited by cell junctions. This provides adherence and stability to the VZ (Hatakeyama et al., 2004; Cappello et al., 2006; Lien et al., 2006a). RGCs act as a self-renewal compartment undergoing symmetric proliferative or asymmetric neurogenic divisions that serve to expand or maintain the pool of RGCs in early development (Chenn and McConnell, 1995; Götz and Huttner, 2005; Buchman and Tsai, 2007). In contrast, IPCs have lost their contact with both apical and basal surfaces and appear as loosely arranged cells whose signs of polarity are apparently lost (Attardo et al., 2008; Noctor et al., 2008). IPCs originate from asymmetric divisions of RGCs in which daughter cells move superficially to the VZ and give rise to the SVZ. Time-lapse imaging studies have revealed that most of the IPCs undergo one single round of symmetric division, while few of them are subjected to a second mitosis that generates one or two pairs of neurons, respectively (Noctor et al., 2004; Haubensak et al., 2004). Therefore, IPCs may be considered to be neurogenic transit amplifying progenitors that expand the pool of differentiated neuronal cells. This process is known as indirect neurogenesis and contrasts with direct neurogenesis that exemplifies neuronal generation directly from RGCs.

The SVZ region enlarges accordingly with cortical expansion during mammalian evolution (Molnár et al., 2006; Noctor et al., 2008). Therefore, an increase in IPCs or in their number of symmetric mitotic cell divisions may have contributed to the tangential expansion of cortical surface that accompanied mammalian brain evolution (Kriegstein et al., 2006; Martínez-Cerdeño et al., 2006). Despite the increased attention on IPCs, the final fate and position of IPCs progeny is unresolved. Two conflicting models suggest IPC contribution exclusively to upper layer cortical neurons (Tarabykin et al., 2001; Cubelos et al., 2007) versus a more general contribution to all cortical layers (Haubensak et al., 2004; Englund et al., 2005).

The molecular mechanisms by which genesis and proliferation of the IPCs are controlled have not been adequately addressed. The activity of the proneural genes Neurogenin2 (*Ngn2*) and *Mash1* have a role in modulating the ratio between apical and basal mitoses during corticogenesis (Miyata et al., 2004; Britz et al., 2006). While at early stages *Ngn2* promotes SVZ cell maturation and neuronal differentiation, later on, its function changes to preventing premature exhaustion of VZ proliferative activity (Britz et al., 2006). It remains unknown how Ngn2 exerts these different functions during cortical neurogenesis and whether Ngn2-independent mechanisms are in place to promote SVZ identity.

IPCs and RGCs also differ in their gene expression profiles. IPCs lack expression of key transcriptional regulators that function in RGC self-renewal, including Pax6, Emx2, and Sox2, while they express Tbr2, Cux1-2, Lmo4, and Svet1 (Englund et al., 2005; Nieto et al., 2004; Cappello et al., 2006; Tarabykin et al., 2001). T-brain-2 (*Tbr2*) gene (NCBI: Eomes), encoding a T box-containing transcriptional regulator closely related to Tbr1, has been widely used as a marker of IPCs. In fact, unlike other IPC markers, Tbr2 transcript and protein are confined to cortical IPCs cells, but not to their progeny, thereby providing a unique molecular tool for unambiguous identification of IPCs (Bulfone et al., 1999; Englund et al., 2005; Hevner et al., 2006). Tbr2 immunohistochemistry has been used extensively to investigate IPC behavior in multiple studies (Cappello et al., 2006; Quinn et al., 2007; Faiz et al., 2008; Yoon et al., 2008). Despite its extensive use as an IPC marker, the role of Tbr2 in IPCs is still poorly understood.

Tbr1 is specifically expressed in early-born neurons of the preplate and layer 6 of the cortical primordium (Bulfone et al., 1995). Interestingly, loss of *Tbr1* results in a defect in corticogenesis leading to preplate splitting defects, radial migration failure, and misspecification of layer 6 and subplate neurons (Hevner et al., 2001). In light of the critical role of Tbr1in neurogenesis, we sought to determine the function of its homolog Tbr2 during cortical development. *Tbr2* mutant embryos arrest their development soon after implantation

when they fail to differentiate trophoblast cell lineage (Russ et al., 2000; Strumpf et al., 2005). To overcome this early lethality and address the function of Tbr2 in later development, we have generated a conditional *Tbr2* allele. In a previous study, we investigated Tbr2's role in retinogenesis and uncovered its unsuspected function in controlling retinal ganglion cell differentiation directly downstream of Pou4f2 (Mao et al., 2008). In this study, we have investigated the role of Tbr2 in cortical IPC specification, function, and developmental potential. Forebrain-specific *Tbr2* mutants exhibit a large decrease in SVZ-proliferating cells and basal cell mitosis, together with loss of IPC-specific gene expression, while RGCs in the VZ did not exhibit any defect. Hence, IPC-dependent indirect neurogenesis promoting neuronal expansion was strikingly affected in *Tbr2* mutant cortices leading to a reduced cortical plate (CP). Interestingly, all cortical layers were affected by loss of IPC progenitors, indicating that IPC-derived neuronal progeny contribute to both deeper and upper cortical layers. These findings were further supported by following $Tbr2^{+}$ IPC cell progeny using a transgenic cell fate reporter. Interestingly, Tbr2 misexpression in the cortex was sufficient to promote IPC fate at the extent of RGC identity and their delay in cell-cycle exit. These results provide evidence that Tbr2 is required for IPC formation and that this transcriptional regulator is sufficient to establish IPC identity.

Results

Conditional Inactivation of *Tbr2* in the Forebrain

To elucidate the function of Tbr2 in cortical IPCs, we used the *Foxg1*-Cre strain to specifically ablate *Tbr2* in the forebrain. We crossed $Tbr2^{flox/flox}$, in which exon-3 is flanked by loxP sites (Mao et al., 2008), with transgenic animals in which the Cre recombinase is knocked in the *Foxg1* locus (Hébert and McConnell, 2000). *Foxg1*-cre animals mediate loxP recombination specifically in the forebrain starting from E9.5 as verified by LacZ expression upon crossing with the ROSA26 reporter line (Hébert and McConnell, 2000; Chen et al., 2006; Zhou et al., 2008). Upon Tbr2 exon-3 cre-mediated excision, a large part of the T box domain is lost, followed by a frame shift between exons II and IV, leading to premature termination of translation and, therefore, creating a complete *Tbr2* loss-of-function allele (Mao et al., 2008). Tbr2 transcripts and protein were undetectable in E12.5 and E14.5 mutant forebrains while readily observed in age-matched wild-type forebrains (Figures 1A, 1B, 1D, and 1E and data not shown). Because $Tbr2^{\Delta flox/-}$; *Foxg1*-Cre mice were lethal at birth, $Tbr2^{\Delta flox/-}$; *Foxg1*-Cre and control ($Tbr2^{+/\Delta flox}$; *Foxg1*-Cre) brains were compared at E18.5.

Dorsal views revealed reduction of cortex size and severely hypoblastic olfactory bulbs of mutants compared to age-matched control brains (Figures 1G and 1H). This reduction in cortical surface was already notable as early as E14.5 (Figures 1C and 1F). Cresyl violet staining of E18.5 coronal brain sections revealed a significant decrease in cortical thickness along all longitudinal and mediolateral cortical areas of mutants (Figures 1I and 1J). On average, the cortical plate (CP) was 40.7% ± 8% thinner, with a reduction of 28.2% ± 5% and 50.2% ± 6% of deeper and upper cortical layers respectively, in mutants with respect to controls (Figure 1O). However, cell density in the CP did not differ significantly between genotypes (WT CP, 8700 ± 700 cells/mm^2; n = 3; Tbr2 mutant CP, 9200 ± 500 cells/mm^2; n = 3), suggesting that the cortical deficit arises from severe cell loss. In addition, we noted severe defects in axonal connectivity in *Tbr2* mutant forebrains, such that all major commissural axonal tracts failed to cross the midline (Figures 1K–1N). The corpus callosum was completely lacking in *Tbr2* mutant brains (Figures 1K and 1M), and L1 staining revealed the formation of Probst bundles, indicating the accumulation of callosal fibers near the midline, but crossing was absent (Figures 1R and 1S). In addition, both anterior and hippocampal commissures were severely defective or absent, as shown by Nissl staining and neurofilament immunohistochemistry (Figures 1L, 1N, 1P, and 1Q). These findings suggest the occurrence

of midline structure defects in forebrain-specific *Tbr2* mutants that have a pivotal role in promoting and guiding the crossing of the axonal projections during development. Further elucidation of the Tbr2-dependent mechanisms leading to such severe axonal navigation will be important for future studies.

Depletion of IPCs in the SVZ of *Tbr2*-Deficient Cortex

The decreased cortical surface and thickness displayed by Tbr2 mutant cortices may be due to reduced cell proliferation, survival, or enhanced neurogenesis. However, consistent with Tbr2-specific expression in IPCs cells, we first investigated IPC development in *Tbr2* mutant forebrains. To assess the number of proliferative cells in S phase in both control and *Tbr2* mutant cortices, BrdU was injected into E15.5 pregnant females and cortices analyzed 1 hr after BrdU pulse. Interestingly, *Tbr2*-deficient cortex displayed an average reduction along the different regions of the cortex of about 22% in $BrdU^+$ cell nuclei, most of which were confined in the most basal area of the periventricular region, corresponding roughly with the SVZ territory (Figures 2A–2C). To identify which cell population was affected in proliferation, immunohistochemistry for the phosphorylated form of histone H3 (PH3) was employed as a marker for cell mitosis and to discriminate between apically or basally located cell divisions corresponding to RGCs or IPC mitotic figures, respectively. We detected a large loss of basal mitosis, corresponding to 74.5% ± 2% loss of IPCs, in E15.5 *Tbr2* mutants versus control cortices (Figures 2D–2F), while the number of mitoses on the apical surfaces was not significantly changed between the two genotypes. Thus, these results imply that *Tbr2* inactivation impairs SVZ residing proliferating cells without affecting ventricular RGCs. Based upon these results, we hypothesized that IPC-specific gene expression should be altered in Tbr2-deficient forebrain.

We next tested expression levels of *Svet1* and *Lmo4* genes, whose expression is specifically confined to IPCs, and *NeuroD1*, which is expressed in IPCs but also differentiating neurons (Cappello et al., 2006; Hevner et al., 2006). As expected, *Svet1*, *Lmo4*, and *NeuroD1* gene expression was strongly downregulated in E15.5 *Tbr2*-deficient cortices (Figures 2G–2L′). To quantify their decreased gene expression levels, we performed qRT-PCR on RNA extracted from isolated E14.5 mutant or WT cortices. Interestingly, all three genes were downregulated in the mutant, with a reduction of 56% ± 5%, 78% ± 3%, and 92% ± 2%, for *NeuroD1*, *Lmo4*, and *Svet1*, respectively (Figure 1M). Furthermore, *Cux2*, another gene known to be expressed by IPCs at this stage, showed a 3-fold reduction in its expression levels (35% ± 6%) (Figure 1M).

IPCs have been identified at the onset of neurogenesis starting from stage E10.0 and are readily detectable by E11.5 (Haubensak et al., 2004; Attardo et al., 2008). Therefore, we wondered whether the generation of IPCs was already impaired in *Tbr2* mutant cortices at early stages. At E10.5, few $Tbr2^+$ IPCs were still detectable, indicating that the protein persisted for some hours after gene excision had occurred (data not shown). Therefore, we decided to focus our analysis on stage E11.5, a stage when no cortical cells were positive for Tbr2 immunohistochemistry (data not shown). At this stage, basal $PH3^+$ IPCs were already significantly reduced in the *Tbr2* mutant background, while no difference was observed in the number of $PH3^+$ apical mitotic figures with respect to controls (Figures 2N–2S). Together, these data reveal a crucial requirement for Tbr2 in the specification and/or maintenance of the IPC pool in the cortical SVZ.

Tbr2-Deficient Cortex Exhibits a Severe Reduction in Neuronal Production

We next investigated how loss of IPCs influences the processes of neuronal commitment and differentiation during early corticogenesis. First, we assessed the amount of β-III-tubulin$^+$ postmitotic neurons in the cortical plate in E11.5 mutant and control cortices. Notably, the

differentiated domain was found consistently enlarged in mutants with respect to WT cortices due to an increased abundance of β-III-tubulin$^+$ (Figures 3A–3D). Moreover, different β-III-tubulin$^+$ neurons were scored within the mutant VZ, while these cells were barely visible at this stage in a WT background (Figures 3E and 3F, arrowheads). These data indicate that premature neuronal differentiation is occurring in Tbr2 mutant cortices, contributing to a thicker cortical plate, starting from early stages of corticogenesis. Combined, these results suggest that mutant RGCs function as neurogenic-founder progenitors beginning in early stages of development and concurrently lose their ability to generate IPCs.

Cortical IPCs are considered transient amplifying progenitors that undergo one or two cell divisions before differentiating into postmitotic cells. In this respect, IPCs represent a secondary and short-lasting source of proliferative progenitors generated by RGC asymmetric divisions, which enable a further step of cell amplification starting from each single RGC. The absence of IPCs from early stages of corticogenesis is therefore predicted to lead to an overall reduction in the number of neuronal differentiated progeny along with cortical development. Consistent with this hypothesis, we detected a reduction of the cortical differentiated tissue as visualized by β-III-tubulin staining (TuJ1) at E13.5, indicating a decreased rate of neuronal production (Figures 3G and 3J). To better visualize this reduction, we employed NeuroD1 immunocytochemistry, which normally highlights the nucleus of differentiated neurons in the intermediate zone (IZ). NeuroD1$^+$ neurons were found to be reduced by about 50% in E14.5 Tbr2-deficient cortices compared to controls (Figures 3H and 3K). To determine whether this reduction in early-born neurons translated into a smaller number of mature and definitive glutamatergic neurons, we used Tbr1 immunohistochemistry for labeling mature early-born neurons and confirmed about 60% loss of the entire Tbr1$^+$ neuronal population in E14.5 mutant with respect to control cortices (Figures 3N, 3O, 3Q, and 3R). While loss of Tbr2 has a dramatic effect on IPCs and their derivatives, we did not detect any major alteration in the quantity, organization, or general polarity of the RGCs residing in the mutant VZ, as highlighted by Pax6, Nestin, Glast, and ZO-1 immunoreactivity (Figures 3T–3W and data not shown). Together, our observations reveal that *Tbr2* inactivation produces an early loss of IPCs that subsequently translates in a reduction in neuronal cell generation detectable both at early (NeuroD$^+$) and late (Tbr1$^+$) stages of neuronal differentiation.

We next sought to determine whether IPC loss in *Tbr2* mutant cortices was due to premature cell death. TUNEL assay and activated caspase-3 immunohistochemistry were performed at E11.5, E13.5, and E14.5 control and Tbr2 mutant cortices (Figures S1A–S1E available online and data not shown). We did not observe a significant change in apoptosis between the two different genotypes. These findings suggest that IPC loss is not due to a failure in maintenance of the IPC cell state, implying that mechanisms in IPC generation could be impaired.

Together, these results indicate that neurogenic asymmetric divisions giving rise to postmitotic young neurons are increased in the *Tbr2* mutant with respect to the control from E11.5 onward. It is therefore likely that *Tbr2* inactivation leads to a shift between progenitor (indirect) and neurogenic (direct) promoting RGC asymmetric divisions, which prevents the production of IPC progenitors and their progeny. Hence, these alterations lead at early stages (E11.5) to a temporary increase in newly generated neurons while, later on, the overall neural production declines due to the loss of the IPC proliferative compartment.

Forebrain-Specific *Tbr2* Mutants Display a Reduced Number of Neurons in Both Deeper and Upper Cortical Layers

Because Tbr2$^{\Delta flox\Delta flox}$; *Foxg1*-Cre embryos reach late stages of embryonic development, we were able to determine how IPC loss affected cortical layer formation and laminar cellular composition. In fact, these mutants offer a unique opportunity to evaluate deficits in cortical laminar shaping as the result of the early loss of IPCs, thus allowing us to examine the direct

contribution of IPC progeny to cortical structures. At E18.5, *Tbr2* mutant cortices displayed a 2-fold reduction in thickness compared to controls, as indicated by Nissl staining and expression of the glutamatergic panneuronal marker *Math2* (*Nex1; NeuroD6*) (Goebbels et al., 2006) (Figures 1I,1J, 4A, and 4B). This result confirmed the neuronal reduction obtained at earlier developmental stages. We therefore investigated whether the observed cortical decrease was achieved by a general neuronal loss affecting all the cortical layers or by a selective reduction in the most superficial layers as suggested by previous studies (Wu et al., 2005; Cubelos et al., 2007). To assess this issue, we employed molecular markers of the different cortical layers, analyzing initially the somatosensory cortical domain. *FoxP2*, *Tle4*, and *ER81* (NCBI: *Etv1*) are expressed by cortico-fugal neurons, and their expression domains are restricted to cortical layers V and VI (Molyneaux et al., 2007; Leone et al., 2008). All three genes showed a reduced expression domain in *Tbr2* mutant with respect to wild-type cortices at E18.5, indicating an overall decrease of deeper cortical layers (Figures 4C–4H). Furthermore, superficial layers were also affected in *Tbr2* mutants, as highlighted by expression of *Rorβ* (layer IV marker) and *Lhx2*, *Satb2*, and *Lmo3* (layer II/III markers), mainly expressed in callosal projecting neurons (Figures 4I–4P). To quantify this neuronal reduction in *Tbr2* mutant cortices, we counted the number of cortico-fugal $Tbr1^+$ or callosal projecting $Satb2^+$ neurons in control and *Tbr2*-deficient somatosensory cortices. In both cases, we detected a large neuronal decrease in *Tbr2* mutants, reaching about 33.6% ± 5% and 59.5% ± 3% reduction for $Tbr1^+$ and $Satb2^+$ neurons, respectively (Figures 4Q–4U). To generalize this defect to the entire *Tbr2* mutant cortex, we performed a detailed gene expression analysis in other cortical domains along the rostrocaudal and mediolateral axes (Figures S2 and S3). These results reveal a general reduction in both deeper and upper cortical layers in medial and lateral cortices (Figures S2 and S3). Although these data indicate that neurons derived from $Tbr2^+$ IPCs contribute to each cortical layer, it still remains possible that the loss of IPCs may cause a non-cell-autonomous effect on differentiating neurons, which would imply an IPC-independent origin. To provide further evidence for a cell-autonomous mechanism at the foundation of the defects displayed by *Tbr2* mutants, we took advantage of BAC transgenic mice expressing *GFP* under the control of the *Tbr2* endogenous regulatory sequences (*Eomes::GFP*; Kwon and Hadjantonakis, 2007). In agreement with previous observations, EGFP activity overlapped with Tbr2 protein localization in the developing cerebral cortex both at early (E11.5) and successive (E14.5) stages of corticogenesis (Figures S4A–S4H). The large majority of the GFP^+ cells expressed the endogenous Tbr2, while only a minority colabeled with the RGC marker Pax6 (Figures S4B, S4E, and S4G). However, due to stability of the GFP protein, the Tbr2::GFP strain can be used as a lineage tracer. We noted many GFP^+ cells localized in the cortical plate, some of them expressing markers of differentiated neurons such as Tbr1 and TuJ1 (Figures S4F and S4H). This result indicates that the progeny of $Tbr2^+$ IPCs maintain gene reporter activity following their differentiation, even if Tbr2 endogenous gene expression is normally suppressed. Using GFP as a molecular tracer of the $Tbr2^+$ cell lineage, we noted that, in newborn *Tbr2::EGFP*-transgenic brains (P0), GFP^+ neurons were found largely distributed across the different cortical layers. In particular, colabeling with Tbr1 (layer V and VI) and Satb2 (mainly layer II/III) showed that many GFP^+ cells are settled in all the layers, with prevalence in the upper cortical layers (Figures S4I–S4K). In summary, these results reveal a significant contribution of the $Tbr2^+$ IPC neuronal progeny to each cortical layer and reveal that loss of IPCs causes a dramatic reduction in cortical cell mass at all cortical levels.

Tbr2 Misexpression Promotes IPC Fate and Inhibits Cell-Cycle Exit

Our results indicate that lack of Tbr2 function leads to a large loss of cortical IPCs, without any notable effect on other cortical cells types. We next investigated whether forced expression of Tbr2 was able to promote IPC fate at the expense of other cortical cell types. Tbr2 misexpression was achieved via in utero electroporation in E13.5 wild-type embryos using a

plasmid construct in which expression of the *Tbr2* coding sequence is under the control of a constitutively active CMV/β-actin promoter with an *IRES-EGFP* element for the identification of electroporated cells (Saito, 2006). Forty-eight hours after electroporation (E15.5), forced expression of *Tbr2* in the RGC territory dramatically affects structural layering of the developmental cortex. In controls electroporated with *EGFP*, we noted normal composition of the three cortical layers (VZ, IZ, and CP) (Figures S5A and S5B); in contrast, Tbr2 misexpression led to an anatomical expansion of the VZ/SVZ region at the extent of the overlaying IZ (Figures S5D and S5E, arrows). In addition, GFP-expressing cells had migrated out of the VZ/SVZ region and displayed a typical bipolar shape, while Tbr2-misexpressing cells exhibited a multipolar-like morphology both in germinal neuroepithelium and in the basal regions of the VZ (Figures S5C and S5F). Since it has been described that SVZ-residing cells have a multipolar morphology (Noctor et al., 2004), we asked whether Tbr2 misexpression induces IPC identity or, alternatively, arrest of neuronal migration leading to cell accumulation within the SVZ. We identified a strong induction in cell proliferation in the *Tbr2*-electroporated site as assessed by 1 hr BrdU incorporation (Figures 5A, 5B, 5D, and 5E). A 2-fold induction of $BrdU^+$ cells was found in the target site, with 46% of the $Tbr2^+$ cell population in cell-cycle S phase (Figures 5C and 5F). Of note, PH3 immunohistochemistry showed that Tbr2 misexpression led to an 8-fold increase in basal mitoses, but a drastic reduction in apical $PH3^+$ cells (Figures 5G–5I). Interestingly, the majority of the basal $PH3^+$ cells were expressing GFP, indicating that Tbr2 increased nonsurface mitoses through a cell-autonomous mechanism (Figures 5H, arrowheads). Further, *Tbr2* forced expression appeared to repress cell-cycle exit, as assessed by quantifying the $Ki67^+/BrdU^-$ cells after 24 hr BrdU incorporation, which were reduced from 14.65% to 10.07% in control with respect to Tbr2-electroporated tissues (Figures 5J–5L). These results showed that Tbr2 misexpression stimulates cell proliferation in the SVZ and inhibits cell-cycle withdrawal. To confirm this hypothesis, gene expression studies with IPC molecular markers such as *Svet1*, *Lmo4*, *Slc17a6* (*Vglut2*), and *NeuroD1* (Cappello et al., 2006) were carried out in E15.5 brain electroporated with *Tbr2* or *EGFP* only 48 hr earlier. In all cases, according with the Tbr2 gene and protein misexpression in the electroporated site (Figures 6A–6D′), IPC gene expression domains were found ectopically expanded in more apical and basal regions (Figures 6E–6L′). Taken together, these results indicate that *Tbr2* exogenous expression is sufficient to force differentiation toward an IP cell fate and, simultaneously, to promote cell soma localization in the SVZ region.

Tbr2 Ectopic Expression Represses RGC Identity, Disarranges VZ, and Causes Non-Cell-Autonomous RGC Differentiation

Enhanced IPC commitment promoted by *Tbr2* exogenous expression could be achieved by an increase in IPC proliferation or, alternatively, by a change in cell-type specification. To test this issue, we found that PH3 immunohistochemistry revealed a severe reduction of apical surface mitoses in the *Tbr2*-elecroporated area, indicating a compromised development of ventricular RGCs (Figures 5G and 5H). The *Pax6* gene, whose expression is restricted to RGCs, was analyzed in the Tbr2 misexpression territory in E15.5 cortices. Surprisingly, we detected focal repression of *Pax6* gene expression and protein coinciding with the *Tbr2*-electroporated domain (Figures 7A–7H). In particular, the few $Pax6^+$ cells still detectable in the periventricular area were not expressing Tbr2, indicating the all the RGCs targeted for Tbr2 exogenous expression lost their RGC identity (Figure 7H). In contrast, *EGFP* ectopic expression did not alter Pax6 protein localization in the VZ and, therefore, several periventricular cells showed Pax6/EGFP double staining (Figures 7C–7E). Loss of RGCs was confirmed by the strong reduction of the RGC-specific markers *Emx2* and *Sox2* in the periventricular expression (Figures 7I–7J′ and data not shown). Since apoptosis in the VZ was not found to be significantly increased upon protracted Tbr2 activation, as tested by TUNEL assay (Figure S6), our data supported an expansion of the IPC population at the expense of RGCs and suggested a change of RGCs cell fate toward an IPC identity.

Notably, we found severe cell disorganization and extensive neuronal differentiation in the periventricular region targeted for Tbr2 misexpression as verified by H&E staining (Figures 7K–7N) and β-III-tubulin (TuJ1), bHLHb5, and Satb2 enhanced immunoreactivity in the VZ (Figures 7O–7W′). This result could be due to the high neurogenic potential of the Tbr2-induced IPCs, which generate postmitotic neurons after a single or a few rounds of cell division. We tested this hypothesis by examining the colocalization between the GFP reporter (Tbr2-misexpressing cells) and the markers of neuron differentiation (data not shown). However, we observed β-III-tubulin^{+}/GFP^{-} cells in the *Tbr2*-targeted area, suggesting that some RGCs are induced to differentiate following a non-cell-autonomous mechanism and are not targeted for Tbr2 misexpression.

RGCs are tightly connected to each other by highly polarized cell junctions located on their apical surface, and loss of cell adherence induced by cell junction impairment leads to a disorganized VZ and premature differentiation (Cappello et al., 2006; Costa et al., 2008). Therefore, we analyzed the morphological arrangement of RGCs in the Tbr2 ectopic expressing VZ domain. Notably, nestin^{+} RGCs appeared in their usual orderly organized radial orientation in the EGFP-electroporated domain, while, upon Tbr2 misexpression, nestin^{+} RGCs displayed a severely disorganized appearance (Figures S7A–S7F). Immunolocalization for proteins mainly restricted to RGC cell junction structures, like Pals1 and β-catenin, were lost or strongly repressed in the electroporated domain (Kosodo et al., 2004) (Figures S7G–S7R). These data suggest that Tbr2 misexpression in the VZ induces general tissue disorganization and cell detachment, likely due to a depletion of RGCs committed to an IPC fate. However, this VZ disarray has a secondary effect on RGCs that do not express the transgene but are simply located next to the Tbr2-misexpressing cells. These RGCs lose cell-cell junction-based adhesiveness and are forced to prematurely detach from the apical surface and, thereafter, to differentiate into βIII-tubulin^{+} neurons. Collectively, these results indicate that Tbr2 misexpression acts in a cell-autonomous mode in directing RGCs toward an IP cell fate, leading to disorganization of the neuroepithelium, which then promotes additional RGC detachment and neuronal differentiation by a non-cell-autonomous mechanism. Both of these processes cooperatively lead to a near-complete depletion of Pax6^{+} RGCs as observed in the *Tbr2*-targeted ventricular area.

Tbr2 Misexpression Influences Definitive Neuronal Fate and Laminar Positioning

Tbr2 gain-of-function promotes IPC identity at the extent of RGCs and inhibits IPC cell-cycle exit. However, it remains open whether this specific cell state promoted by enhanced Tbr2 activity is competent to regulate neuronal differentiation and generate functional neurons with proper localization in the corresponding cortical layers. To address this issue, we sought to determine the long-term fate of Tbr2 and GFP misexpressing and control cells by electroporating *Tbr2* or *EGFP* plasmids in utero at E12.5 and analyzing their position at E18.5 (Figures 8A and 8B). This strategy allowed us to target proliferating RGC cells normally fated to differentiate into deep cortical residing mature neurons. Accordingly, *EGFP* electroporation at E12.5 labeled a cohort of neurons residing in deeper parts of the cortex and co-expressing the layer VI molecular marker Tbr1 at E18.5 (Figures 8C–8E). In contrast, a large fraction of *Tbr2*-electroporated cells were found localized in more superficial cortical positions, and many of them were found expressing the upper-layer molecular determinant Satb2 (Figures 8F–8H). Improper laminar positioning of the Tbr2-misexpressing cells may be dependent on alterations in neural proliferation or migration activity. To address this issue, BrdU was injected either at E13.5 or E15.5 after electroporation of *GFP* or *Tbr2* at E12.5. This procedure enabled us to label those neurons that normally contribute to deeper or upper cortical layers and also to determine the time point at which Tbr2-misexpressing neuroblasts withdrew from the cell cycle. We found that the majority of the neurons targeted for exogenous *Tbr2* expression and located in more superficial layers stained positive for BrdU when administrated at E15.5, but

not at E13.5 (Figure 8I and 8J). These results indicate that Tbr2 misexpression is able to sustain proliferation activity and/or prevent cell-cycle withdrawal for a specific period of time, influencing the successive events of neuronal cell-type specification and laminar positioning.

Discussion

The identification of the genetic determinants controlling the sequential specification of RGCs, IPCs, and postmitotic neurons in the cerebral cortex is a formidable task that attempts to reveal the critical molecular steps that guide cell specification in the developing cortex. Tbr2 is known to be specifically expressed in the IPC population; nonetheless, its biological function has remained poorly understood. Our results indicate that Tbr2 is strictly required for IPC specification and proliferation. Tbr2 loss of function leads to a dramatic loss of cortical IPCs and their differentiated progenies. This outcome is not due to defects in IPC maintenance, but to a failure in specification. In contrast, genesis, proliferation, and cellular architecture of RGCs were uncompromised in *Tbr2* mutants. Remarkably, in early *Tbr2* mutant cortices (E11.5), we found a temporary increase in differentiated neuronal progenies both in the CP and VZ, when the number of IPCs is already strongly decreased. This implies that RGCs lose their ability to generate IPCs while simultaneously increasing the rate of neuronal production. Taken together, these data strongly suggest that RGCs undergo a switch from progenitor (indirect) to neurogenic (direct) asymmetric divisions. This shift from indirect to direct neurogenesis leads to an increase in neuronal production, together with the loss of IPCs, as we observed in E11.5 *Tbr2* mutant cortex. Afterward, beginning in the middle stages of corticogenesis, this switch in cell division output could account for the remarkable loss of differentiated cortical tissue readily observed in *Tbr2* mutants. In fact, the IPC loss is associated with an absence in transient amplifying cells, which, through symmetric divisions in the SVZ region, amplifies the final neuronal production output.

The assessment of the long-term effects of IPC loss in late embryonic stages, coupled with cell fate lineage analysis performed with *Tbr2*::EGFP transgenic animals, provided us the unique opportunity to reveal the contribution of IPCs to the establishment of mature cortical structures. Surprisingly, we found a general reduction of cortical differentiated tissue elicited by a similar neuronal loss affecting all the cortical layers. These findings are in contradiction with some previous reports regarding the selective contribution of IPCs to the cortical upper layers. This hypothesis was initially based on gene expression studies following the expression in the mature cortex of SVZ-specific molecular markers (Tarabykin et al., 2001; Nieto et al., 2004). However, gene expression studies, although initially suggestive, still remain a descriptive tool when applied to cell lineage analysis. A recent study provided an elegant cell lineage tracing of Math2/Nex-expressing cells by means of Cre-loxP technology (Wu et al., 2005). In this work, clonal analysis of SVZ-residing Math2$^+$ cells showed selective generation of upper-layer cortical neurons (Wu et al., 2005). However, Math2 is expressed only by a fraction of proliferative IPCs and only partially colocalizes with Tbr2. Moreover, lineage tracing has been characterized starting only from E14.5 but not at earlier time points. Therefore, this type of analysis could have analyzed only a fraction of all entire cell progenies generated by IPCs. In this context, it is important to note that Tbr2$^+$ cells appear particularly early in corticogenesis, starting from E10.5 in mouse (Noctor et al., 2008). In addition to cortical deficits, perinatal *Tbr2* mutant brains displayed severely reduced olfactory bulbs. Tbr2 expression has been detected in mitral cells of the differentiated olfactory bulbs and their progenitors during development (Bulfone et al., 1999). Therefore, it is conceivable that *Tbr2* mutant hypoblastic olfactory bulbs might originate from a failure in correct development of mitral cells, as suggested by the loss of reelin and Id-2 expression, two well-known markers of these projection neurons (A.S. and V.B., unpublished data).

Recently, Tbr2 function has been investigated during early embryo development in gastrulation and formation of the germinal layers (Arnold et al., 2008a). Interestingly, Tbr2 was found to be required for correct delamination and migration of the epiblast cells in order to promote mesoderm formation through epithelium-to-mesenchimal transition (EMT). These defects are associated with failure in downregulating E-cadherin expression and maintaining cell junction integrity, suggesting that Tbr2 acts as an upstream repressor of E-cadherin (Arnold et al., 2008a). These findings provide some insight into the cellular processes involved in the development of the cortical neuroepithelium and suggest additional roles for Tbr2 function. In fact, adherence junction ability in mediating RGC adhesion is controlled by cadherin signaling. Mutant cerebral cortices for *N-cadherin* and *α*- or *β-catenin* are strongly impaired and show disorganized RGCs with loss of cell adherence and detachment from the ventricular surface (Junghans et al., 2005; Lien et al., 2006a, 2006b; Kadowaki et al., 2007). Therefore, it is possible that Tbr2 acts in repressing adherence formation in those RGCs daughter cells that are fated to leave the ventricular layer to become IPCs. Hence, Tbr2 would regulate a critical aspect of IPC formation as the delamination from the VZ layer to migrate outward in more basal positions. Nonetheless, it is doubtful that this is the only function of Tbr2 in this context. In fact, it has been widely shown that postmitotic neurons are generated by RGC asymmetric division and cell detachment from ventricular surface (Chenn and McConnell, 1995; Noctor et al., 2004). Therefore, we favor the hypothesis that Tbr2 may early on influence RGC detachment by negatively regulating cell junction signaling, but thereafter directs IPC identity using still unknown molecular mechanisms.

Recently, it has been shown that IPCs may positively influence RGC state maintenance and proliferation stability by acting as Notch-ligand-presenting cells and, therefore, activating the Notch signaling pathway in RGCs and thereby ensuring their stem cell features (Kawaguchi et al., 2008; Yoon et al., 2008). However, although *Tbr2* mutant cortices display a severe reduction of IPCs, we have not detected a major defect in RGC proliferation (PH3 staining and BrdU incorporation) or morphology (Nestin and GLAST immunoreactivity). Therefore, although minor alterations in RGC could not be excluded, it appears that Notch signaling is still mostly preserved in Tbr2 mutant cortices, at least in its non-cell-autonomous effects, as supported by correct expression of the Notch effector genes *Hes1-5* genes (A.S. and V.B., unpublished data). This is probably due to cell types other than IPCs acting like Notch-ligand-presenting cells, as for instance all the young generated neurons confined to the VZ that resulted unaffected in the *Tbr2* mutant background (Yoon et al., 2008).

Marked microcephaly has been shown to arise from silencing of the human *TBR2* ortholog (NCBI:EOMES) caused by an homozygous balanced translocation between chromosomes 3p and 10q (Baala et al., 2007). Microcephalic *TBR2*-deficient brains also display other neuroanatomical malformations, including complete agenesis of the corpus callosum. These defects are strikingly similar to those that we have described in *Tbr2* mutant mouse cortices. In light of our current results, it would be valuable to assess whether *TBR2* mutations lead to a general failure of midline axonal tract crossing as described for mouse brain mutants. Interestingly, *TBR2*-dependent microcephaly is accompanied by reduced cerebellar size, which is consistent with Tbr2's role in the development of deep cerebellar nuclei and unipolar brushes cells (Fink et al., 2006). Notably, *Tbr2*-specific brain inactivation has been recently achieved by another group, crossing Tbr2 conditional mutants with a *Sox1*-Cre mouse line, leading to mutant mice with microcephaly, mild reduction of SVZ cortical progenitors, altered behavior, and reduced dentate gyrus (Arnold et al., 2008b). However, in this case corpus callosum was only marginally affected, and the absence of Tbr2 was associated with the loss of upper cortical neurons only. We propose that agenesis of the corpus callosum is likely due to a defect in axonal guidance, consistent with the formation of Probst bundles in both *Tbr2*-deficient brains and *Tbr2*-specific expression in the midline zipper glia cells (A.S. and V.B., unpublished data).

Our results highlight an evolutionary conserved role for Tbr2 function in establishing correct cerebral cortex expansion and supporting correct development of specific brain structures. In addition, these studies revealed how loss of proper IPC proliferation is a critical cellular process that may lead to human microcephalic syndromes. Therefore, identification of other genes that affect the same cellular processes may reveal additional candidates for the genetic determinants of microcephaly and other diseases.

In conclusion, we have established that Tbr2 is a key molecular determinant of IPC identity, proliferation, and correct differentiation. Particularly striking is Tbr2's ability to impose IPC commitment on to RGCs, leading to formation of SVZ ectopic regions in the proliferative neuroepithelium. Future studies will be needed to unravel the specific Tbr2-dependent molecular network that mediates its role in finely controlling RGC to IPC cellular conversion over time.

Experimental Procedures

Animals and Tissue Preparation

Tbr2 conditional mutant mice ($Tbr2^{flox/flox}$) (Mao et al., 2008) were maintained by backcrossing with C57Bl/6 animals. To inactivate *Tbr2* in the developing forebrain, $Tbr2^{flox/flox}$ mice were crossed with $Tbr2^{\Delta flox/+}$; *Foxg1*-Cre animals (Hébert and McConnell, 2000). Genotyping to distinguish wild-type, floxed, and deleted *Tbr2* alleles was performed as described previously (Mao et al., 2008). Mice were maintained at the San Raffaele Scientific Institute Institutional mouse facility, and experiments were performed in accordance with experimental protocols approved by local Institutional Animal Care and Use Committees (IACUC).

In Situ RNA Hybridization

ISHs on frozen sections were performed as previously described by Schaeren-Wiemers and Gerfin-Moser (1993) with the following modifications. Sections were fixed for 30 min at room temperature in 4% paraformaldeyde in PBS and treated for 5 min with 1 μg/ml proteinase K in 1 mM EDTA, 20 mM Tris-HCl (pH 7.0). Prior to hybridization, they were washed twice in 2× SSC for 15 min and incubated in 0.1 M Tris/0.1 M glycine for at least 30 min. The hybridization solution (60 μl/slide) contained 50% formamide, 5× SSC (pH adjusted with citric acid to pH 6.0), 5% dextran sulfate, 2 mg/ml heparin, 100 μg/ml tRNA, and from 1:100 to 1:50 dilution of the riboprobes, and was performed overnight at 65°C under coverslips. Next, the sections were washed for 1–2 hr in 0.5× SSC, 20% formamide at 65°C. Subsequently, they were treated with 10 μg/ml RNaseA for 30 min at 37°C in NTE, then washed for 4 hr in 0.5× SSC, 20% formamide at 65°C and for 30 min in 2× SSC, and blocked for 1 hr at room temperature in 1% blocking reagent (Roche, Switzerland) in MABT. A 1:5000 dilution of anti-digoxigenin-AP conjugated antibody (Roche) was pre-incubated for at least 1 hr in 1% blocking reagent in MABT at 4°C. Slices were incubated with the antibody overnight at 4°C, washed for 6 hr in TBST, for 30 min in NTMT, and stained using centrifuged BM purple AP substrate (Roche) in 0.3% Tween-20 for 12–36 hr at 4°C or room temperature. They were washed in NTMT, then in distillated water, and mounted in Aquamount (Polysciences). The following probes were used: Svet1, Vglut2, Tis21 (Cappello et al., 2006) (kindly provided by M. Gotz), Math2, and NeuroD1 (Mattar et al., 2008) (kind gift of C. Schuurmans).

Immunohistochemistry

Immunohistochemical analyses were performed as described previously (Colombo et al., 2004). Briefly, frozen or paraffin sections were boiled in 10 mM sodium citrate, pH 6.0, and blocked in 10% normal goat serum (NGS) and 0.2% Triton X-100 for 1 hr at room temperature. Incubation with primary antibodies was performed at 4°C overnight. Secondary antibodies

were applied to sections for 2 hr at room temperature. The primary antibodies utilized were as follows: rabbit anti-Tbr2 (1:300, Chemicon), rabbit anti-Tbr1 (1:400, Chemicon), guinea-pig anti-neuroD1 (1:3000, Santa Cruz), rabbit anti-β-III-tubulin (TuJ1) (1:1000, Covance), rabbit anti-PH3 (1:200, Chemicon), mouse anti-BrdU (1:100, Beckton-Dickinson), rabbit anti-Pax6 (1:300, Covance), mouse anti-β-catenin (1:100, Chemicon), rabbit anti-neurofilament H (200 kDa) (1:500, Chemicon), rabbit anti-Ki67 (1:100, Novocastra), rabbit anti-L1 (1:50, Chemicon), rabbit anti-Pals1 (gift from J. Wijnholds, Netherlands Institute for Neuroscience, The Netherlands). Secondary antibodies were conjugates of Alexa Fluor 488, Alexa Fluor 594, and Alexa Fluor 647 (1:500). DAPI (4′,6′-diamidino-2-phenylindole) was used as nuclear counterstaining. Finally, slices were washed and mounted in Fluorescent Mounting Medium (Dako Cytomation).

Real-Time Quantitative RT-PCR

RNeasy mini-kit (QIAGEN) was used for total RNA isolation and superscript reverse transcriptase II (Invitrogen) for cDNA synthesis starting with 4 μg of total RNA. qPCR was performed with Stratagene Mx3000P using SYBR green master mix (BioRad). Samples were quantified through a standard curve based method; each sample was run in triplicate and normalized to the expression of the housekeeping gene β-actin. Gene expression was assessed in two mutant and WT cortices. Primers used for amplification are shown in Table S1.

In Utero Electroporations

Tbr2 coding sequence (kind gift of J. Rubenstein and A. Bulfone) was cloned in the pCAG (Niwa et al., 1991) expression vector upstream to an *IRES-EGFP* cassette. Electroporation was used to deliver expression vectors to the ventricular RGCs in utero as previously described (Saito, 2006; Gal et al., 2006). Briefly, uterine horns of E12.5 or E13.5 pregnant dams were exposed by midline laparotomy after anesthetization with Avertin (312 mg/kg). 1 μl of DNA plasmid corresponding to 3 μg mixed with 0.03% fast-green dye in PBS was injected in the telencephalic vesiscle using a pulled micropipette through the uterine wall and amniotic sac. 7 mm platinum tweezer-style electrodes were placed outside the uterus over the telencephalon and four pulses of 42 mV were applied at 400 ms intervals by using a BTX square wave electroporator. The uterus was then replaced within the abdomen, the cavity was filled with warm sterile PBS, and the abdominal muscle and skin incisions were closed with silk sutures.

Quantifications and Statistical Analysis

At least three serial sections from three different animals for each genotype were photographed using a Nikon Eclipse 600 fluorescent microscope. For cell density analysis on E18.5 cortical plate, three different images of layers II-II, V, and IV, respectively, were examined for each section. Images were imported into Photoshop CS3. EGFP-only, marker-only, and/or double-positive cells were overlayed manually by color-coded dots in new layers. The number of labeled cells (dots) was calculated using the Record measurements of Photoshop CS3 and imported into Excel 2008. The percentage of labeled cells per region per section was calculated for each brain, and the final mean percentage calculated across all brains. Results were expressed as mean value ± SD and were tested for statistical significance by the one-tailed Student's t test for paired differences with GraphPad Prism software.

Supplementary Material

Refer to Web version on PubMed Central for supplementary material.

Acknowledgments

We thank John Rubenstein, Luca Muzio, and Giorgio Merlo for critical reading of the manuscript and insightful comments. We gratefully acknowledge John Rubenstein, Michelle Studer, Magdalena Gotz, Carol Schuurmans, Victor Tarabykin, Rudolf Grosschedl, Jan Wijnholds, and Susan McConnell for generously providing reagents and mice. Ping Pan is acknowledged for maintaining and genotyping transgenic mouse strains. This work was supported by the Telethon (GGP07181) to V.B., the NIH (RO10HD052115) to A.-K.H, and the National Eye Institute (EY011930 and EY010608-139005) and the Robert A. Welch Foundation (G-0010) to W.H.K.

References

Arnold SJ, Hofmann UK, Bikoff EK, Robertson EJ. Pivotal roles for eomesodermin during axis formation, epithelium-to-mesenchyme transition and endoderm specification in the mouse. Development 2008a;135:501–511. [PubMed: 18171685]

Arnold SJ, Huang GJ, Cheung AF, Era T, Nishikawa S, Bikoff EK, Molnár Z, Robertson EJ, Groszer M. The T-box transcription factor Eomes/Tbr2 regulates neurogenesis in the cortical subventricular zone. Genes Dev 2008b;22:2479–2484. [PubMed: 18794345]

Attardo A, Calegari F, Haubensak W, Wilsch-Bräuninger M, Huttner WB. Live imaging at the onset of cortical neurogenesis reveals differential appearance of the neuronal phenotype in apical versus basal progenitor progeny. PLoS ONE 2008;3:e2388. [PubMed: 18545663]

Baala L, Briault S, Etchevers HC, Laumonnier F, Natiq A, Amiel J, Boddaert N, Picard C, Sbiti A, Asermouh A, et al. Homozygous silencing of T-box transcription factor EOMES leads to microcephaly with polymicrogyria and corpus callosum agenesis. Nat Genet 2007;39:454–456. [PubMed: 17353897]

Britz O, Mattar P, Nguyen L, Langevin LM, Zimmer C, Alam S, Guillemot F, Schuurmans C. A role for proneural genes in the maturation of cortical progenitor cells. Cereb Cortex 2006;16:i138–i151. [PubMed: 16766700]

Buchman JJ, Tsai LH. Spindle regulation in neural precursors of flies and mammals. Nat Rev Neurosci 2007;8:89–100. [PubMed: 17228329]

Bulfone A, Smiga SM, Shimamura K, Peterson A, Puelles L, Rubenstein JL. T-brain-1:a homolog of Brachyury whose expression defines molecularly distinct domains within the cerebral cortex. Neuron 1995;15:63–78. [PubMed: 7619531]

Bulfone A, Martinez S, Marigo V, Campanella M, Basile A, Quaderi N, Gattuso C, Rubenstein JL, Ballabio A. Expression pattern of the Tbr2 (Eomesodermin) gene during mouse and chick brain development. Mech Dev 1999;84:133–138. [PubMed: 10473127]

Bystron I, Blakemore C, Rakic P. Development of the human cerebral cortex: Boulder Committee revisited. Nat Rev Neurosci 2008;9:110–122. [PubMed: 18209730]

Cappello S, Attardo A, Wu X, Iwasato T, Itohara S, Wilsch-Bräuninger M, Eilken HM, Rieger MA, Schroeder TT, Huttner WB, et al. The Rho-GTPase cdc42 regulates neural progenitor fate at the apical surface. Nat Neurosci 2006;9:1099–1107. [PubMed: 16892058]

Chen L, Liao G, Yang L, Campbell K, Nakafuku M, Kuan CY, Zheng Y. Cdc42 deficiency causes Sonic hedgehog-independent holoprosencephaly. Proc Natl Acad Sci USA 2006;103:16520–16525. [PubMed: 17050694]

Chenn A, McConnell SK. Cleavage orientation and the asymmetric inheritance of Notch1 immunoreactivity in mammalian neurogenesis. Cell 1995;82:631–641. [PubMed: 7664342]

Colombo E, Galli R, Cossu G, Gécz J, Broccoli V. Mouse orthologue of ARX, a gene mutated in several X-linked forms of mental retardation and epilepsy, is a marker of adult neural stem cells and forebrain GABAergic neurons. Dev Dyn 2004;231:631–639. [PubMed: 15376319]

Costa MR, Wen G, Lepier A, Schroeder T, Gotz M. Par-complex proteins promote proliferative progenitor divisions in the developing mouse cerebral cortex. Development 2008;135:11–22. [PubMed: 18032449]

Cubelos B, Sebastián-Serrano A, Kim S, Moreno-Ortiz C, Redondo JM, Walsh CA, Nieto M. Cux-2 controls the proliferation of neuronal intermediate precursors of the cortical subventricular zone. Cereb Cortex 2007;18:1758–1770. [PubMed: 18033766]

Englund C, Fink A, Lau C, Pham D, Daza RA, Bulfone A, Kowalczyk T, Hevner RF. Pax6, Tbr2, and Tbr1 are expressed sequentially by radial glia, intermediate progenitor cells, and postmitotic neurons in developing neocortex. J Neurosci 2005;25:247–251. [PubMed: 15634788]

Faiz M, Acarin L, Villapol S, Schulz S, Castellano B, Gonzalez B. Substantial migration of SVZ cells to the cortex results in the generation of new neurons in the excitotoxically damaged immature rat brain. Mol Cell Neurosci 2008;38:170–182. [PubMed: 18434192]

Fink AJ, Englund C, Daza RA, Pham D, Lau C, Nivison M, Kowalczyk T, Hevner RF. Development of the deep cerebellar nuclei: transcription factors and cell migration from the rhombic lip. J Neurosci 2006;26:3066–3076. [PubMed: 16540585]

Gal JS, Morozov YM, Ayoub AE, Chatterjee M, Rakic P, Haydar TF. Molecular and morphological heterogeneity of neural precursors in the mouse neocortical proliferative zones. J Neurosci 2006;26:1045–1056. [PubMed: 16421324]

Goebbels S, Bormuth I, Bode U, Hermanson O, Schwab MH, Nave KA. Genetic targeting of principal neurons in neocortex and hippocampus of NEX-Cre mice. Genesis 2006;44:611–621. [PubMed: 17146780]

Götz M, Huttner WB. The cell biology of neurogenesis. Nat Rev Mol Cell Biol 2005;6:777–788. [PubMed: 16314867]

Hatakeyama J, Bessho Y, Katoh K, Ookawara S, Fujioka M, Guillemot F, Kageyama R. Hes genes regulate size, shape and histogenesis of the nervous system by control of the timing of neural stem cell differentiation. Development 2004;131:5539–5550. [PubMed: 15496443]

Haubensak W, Attardo A, Denk W, Huttner WB. Neurons arise in the basal neuroepithelium of the early mammalian telencephalon: a major site of neurogenesis. Proc Natl Acad Sci USA 2004;101:3196–3201. [PubMed: 14963232]

Hébert JM, McConnell SK. Targeting of cre to the Foxg1 (BF-1) locus mediates loxP recombination in the telencephalon and other developing head structures. Dev Biol 2000;222:296–306. [PubMed: 10837119]

Hevner RF, Shi L, Justice N, Hsueh Y, Sheng M, Smiga S, Bulfone A, Goffinet AM, Campagnoni AT, Rubenstein JL. Tbr1 regulates differentiation of the preplate and layer 6. Neuron 2001;29:353–366. [PubMed: 11239428]

Hevner RF, Hodge RD, Daza RA, Englund C. Transcription factors in glutamatergic neurogenesis: conserved programs in neocortex, cerebellum, and adult hippocampus. Neurosci Res 2006;55:223–233. [PubMed: 16621079]

Junghans D, Hack I, Frotscher M, Taylor V, Kemler R. Beta-catenin-mediated cell-adhesion is vital for embryonic forebrain development. Dev Dyn 2005;233:528–539. [PubMed: 15844200]

Kadowaki M, Nakamura S, Machon O, Krauss S, Radice GL, Takeichi M. N-cadherin mediates cortical organization in the mouse brain. Dev Biol 2007;304:22–33. [PubMed: 17222817]

Kawaguchi A, Ikawa T, Kasukawa T, Ueda HR, Kurimoto K, Saitou M, Matsuzaki F. Single-cell gene profiling defines differential progenitor subclasses in mammalian neurogenesis. Development 2008;135:3113–3124. [PubMed: 18725516]

Kosodo Y, Roper K, Haubensak W, Marzesco AM, Corbeil D, Huttner WB. Asymmetric distribution of the apical plasma membrane during neurogenic divisions of mammalian neuroepithelial cells. EMBO J 2004;23:2314–2324. [PubMed: 15141162]

Kriegstein AR, Götz M. Radial glia diversity: a matter of cell fate. Glia 2003;43:37–43. [PubMed: 12761864]

Kriegstein A, Noctor S, Martínez-Cerdeño V. Patterns of neural stem and progenitor cell division may underlie evolutionary cortical expansion. Nat Rev Neurosci 2006;7:883–890. [PubMed: 17033683]

Krubitzer L. The magnificent compromise: cortical field evolution in mammals. Neuron 2007;56:201–208. [PubMed: 17964240]

Kwon GS, Hadjantonakis AK. Eomes:GFP-a tool for live imaging cells of the trophoblast, primitive streak, and telencephalon in the mouse embryo. Genesis 2007;45:208–217. [PubMed: 17417802]

Leone DP, Srinivasan K, Chen B, Alcamo E, McConnell SK. The determination of projection neuron identity in the developing cerebral cortex. Curr Opin Neurobiol 2008;18:28–35. [PubMed: 18508260]

Lien WH, Klezovitch O, Fernandez TE, Delrow J, Vasioukhin V. alphaE-catenin controls cerebral cortical size by regulating the hedgehog signaling pathway. Science 2006a;311:1609–1612. [PubMed: 16543460]

Lien WH, Klezovitch O, Vasioukhin V. Cadherin-catenin proteins in vertebrate development. Curr Opin Cell Biol 2006b;18:499–506. [PubMed: 16859905]

Mao CA, Kiyama T, Fururta Y, Hadjantonakis AK, Klein WH. Eomesodermin, a target gene of Pou4f2, is required for retinal ganglion cell and optic nerve development in the mouse. Development 2008;135:271–280. [PubMed: 18077589]

Martínez-Cerdeño V, Noctor SC, Kriegstein AR. The role of intermediate progenitor cells in the evolutionary expansion of the cerebral cortex. Cereb Cortex 2006;16:i152–i161. [PubMed: 16766701]

Mattar P, Langevin LM, Markham K, Klenin N, Shivji S, Zinyk D, Schuurmans C. Basic helix-loop-helix transcription factors cooperate to specify a cortical projection neuron identity. Mol Cell Biol 2008;28:1456–1469. [PubMed: 18160702]

Miyata T, Kawaguchi A, Saito K, Kawano M, Muto T, Ogawa M. Asymmetric production of surface-dividing and non-surface-dividing cortical progenitor cells. Development 2004;131:3133–3145. [PubMed: 15175243]

Molnár Z, Métin C, Stoykova A, Tarabykin V, Price DJ, Francis F, Meyer G, Dehay C, Kennedy H. Comparative aspects of cerebral cortical development. Eur J Neurosci 2006;23:921–934. [PubMed: 16519657]

Molyneaux BJ, Arlotta P, Menezes JR, Macklis JD. Neuronal subtype specification in the cerebral cortex. Nat Rev Neurosci 2007;8:427–437. [PubMed: 17514196]

Monuki ES, Walsh CA. Mechanisms of cerebral cortical patterning in mice and humans. Nat Neurosci 2001;4:1199–1206. [PubMed: 11687830]

Nieto M, Monuki ES, Tang H, Imitola J, Haubst N, Khoury SJ, Cunningham J, Gotz M, Walsh CA. Expression of Cux-1 and Cux-2 in the subventricular zone and upper layers II-IV of the cerebral cortex. J Comp Neurol 2004;479:168–180. [PubMed: 15452856]

Niwa H, Yamamura K, Miyazaki J. Efficient selection for high-expression transfectants with a novel eukaryotic vector. Gene 1991;108:193–199. [PubMed: 1660837]

Noctor SC, Martínez-Cerdeño V, Ivic L, Kriegstein AR. Cortical neurons arise in symmetric and asymmetric division zones and migrate through specific phases. Nat Neurosci 2004;7:136–144. [PubMed: 14703572]

Noctor SC, Martínez-Cerdeño V, Kriegstein AR. Distinct behaviors of neural stem and progenitor cells underlie cortical neurogenesis. J Comp Neurol 2008;508:28–44. [PubMed: 18288691]

Quinn JC, Molinek M, Martynoga BS, Zaki PA, Faedo A, Bulfone A, Hevner RF, West JD, Price DJ. Pax6 controls cerebral cortical cell number by regulating exit from the cell cycle and specifies cortical cell identity by a cell autonomous mechanism. Dev Biol 2007;302:50–65. [PubMed: 16979618]

Rakic P. Developmental and evolutionary adaptations of cortical radial glia. Cereb Cortex 2000;13:541–549. [PubMed: 12764027]

Rakic P. A century of progress in corticoneurogenesis: from silver impregnation to genetic engineering. Cereb Cortex 2006;16:3–17.

Russ AP, Wattler S, Colledge WH, Aparicio SA, Carlton MB, Pearce JJ, Barton SC, Surani MA, Ryan K, Nehls MC, et al. Eomesodermin is required for mouse trophoblast development and mesoderm formation. Nature 2000;404:95–99. [PubMed: 10716450]

Saito T. In vivo electroporation in the embryonic mouse central nervous system. Nat Protocols 2006;1:1552–1558.

Schaeren-Wiemers N, Gerfin-Moser A. protocol to detect transcripts of various types and expression levels in neural tissue and cultured cells: in situ hybridization using digoxigenin-labelled cRNA probes. Histochemistry 1993;100:431–440. [PubMed: 7512949]

Strumpf D, Mao CA, Yamanaka Y, Ralston A, Chawengsaksophak K, Beck F, Rossant J. Cdx2 is required for correct cell fate specification and differentiation of trophectoderm in the mouse blastocyst. Development 2005;132:2093–2102. [PubMed: 15788452]

Tarabykin V, Stoykova A, Usman N, Gruss P. Cortical upper layer neurons derive from the subventricular zone as indicated by Svet1 gene expression. Development 2001;128:1983–1993. [PubMed: 11493521]

Wu SX, Goebbels S, Nakamura K, Nakamura K, Kometani K, Minato N, Kaneko T, Nave KA, Tamamaki N. Pyramidal neurons of upper cortical layers generated by NEX-positive progenitor cells in the subventricular zone. Proc Natl Acad Sci USA 2005;102:17172–17177. [PubMed: 16284248]

Yoon KJ, Koo BK, Im SK, Jeong HW, Ghim J, Kwon MC, Moon JS, Miyata T, Kong YY. Mind bomb 1-expressing intermediate progenitors generate notch signaling to maintain radial glial cells. Neuron 2008;58:519–531. [PubMed: 18498734]

Zhou L, Bar I, Achouri Y, Campbell K, De Backer O, Hebert JM, Jones K, Kessaris N, de Rouvroit CL, O'Leary D, et al. Early forebrain wiring: genetic dissection using conditional Celsr3 mutant mice. Science 2008;320:946–949. [PubMed: 18487195]

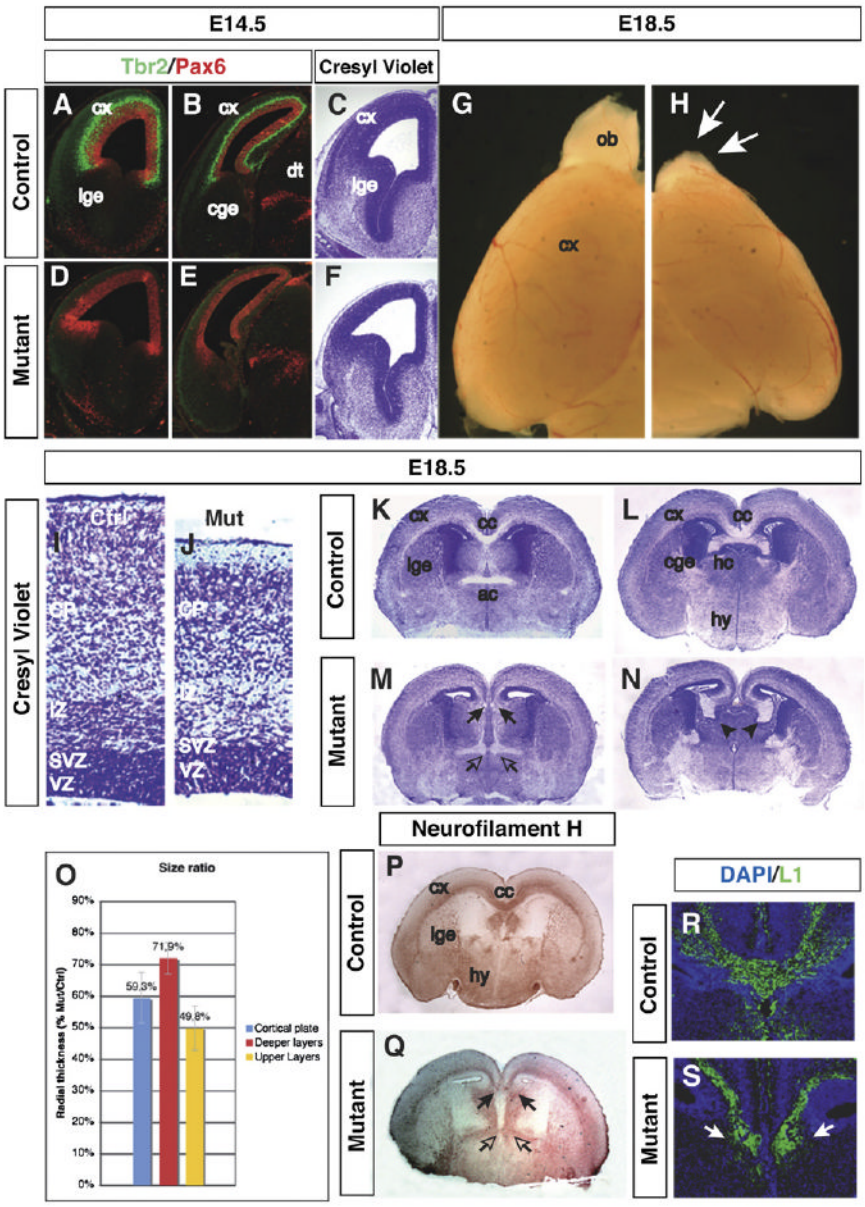

Figure 1. Forebrain-Specific *Tbr2* Ablation Leads to Reduced Cerebral Cortex, Hypoblastic Olfactory Bulbs, and Failure in Major Axonal Commissural Tract Formation

(A, B, D, and E) Immunohistochemistry for Tbr2 (green) and Pax6 (red) in E14.5 forebrain coronal sections of control (*Tbr2*$^{+/\Delta flox}$; *Foxg1*-Cre) (A and B) and *Tbr2* mutants (*Tbr2*$^{\Delta flox/\Delta flox}$; *Foxg1*-Cre) (D and E). Note the complete loss of Tbr2 protein staining in the forebrain-specific *Tbr2* mutant cortex (D and E).

(C and F) Cresyl violet staining of rostral coronal sections of E14.5 control (C) and *Tbr2* mutant (F) cortices showing the first time point at which a morphological reduction of the cortical surface in *Tbr2* mutants with respect to controls is noticeable.

(G and H) E18.5 *Tbr2* mutant brains have a notable reduction in cortical tissue with respect to control and severe hypoblastic olfactory bulbs (arrows). (I and J) Cresyl violet staining of coronal sections through the cerebral cortex highlighting a reduction in the cortical wall tissue in *Tbr2* mutants compared to controls.

(K–N) Coronal sections through the brains of control and *Tbr2* mutant forebrains reveal the failure or strong impairment of commissural axonal tracts to cross the midline. Corpus callosum (arrows) and anterior (empty arrows) and hippocampal (arrowheads) commissures are strongly compromised in *Tbr2* mutants (M and N).

(O) Quantitative measurement of the reduction of the overall mutant cortical thickness (blue bar) and of the deeper (IV and V) and upper (IV, III-II) layers (red and yellow bars, respectively) with respect to relative controls at E18.5 (n = 3, each genotype).

(P and Q) Neurofilament H (200 kDa) immunohistochemistry confirms the histological analysis results, revealing a specific impairment of callosal and commissural axon to cross the midline brain structures.

(R and S) Higher-magnification images of the control (R) and Tbr2 mutant (S) corpus callosum in the midline region stained with an L1 antibody. Note that Tbr2 mutant $L1^+$ callosal projections failed to cross the midline forming the Proust bundles (arrows).

ac, anterior commissure; cc, corpus callosum; cge, caudal ganglionic eminence; cx, cerebral cortex; dt, dorsal thalamus; hc, hippocampal commissure; hy, hypothalamus; lge, lateral ganglionic eminence; ob, olfactory bulb.

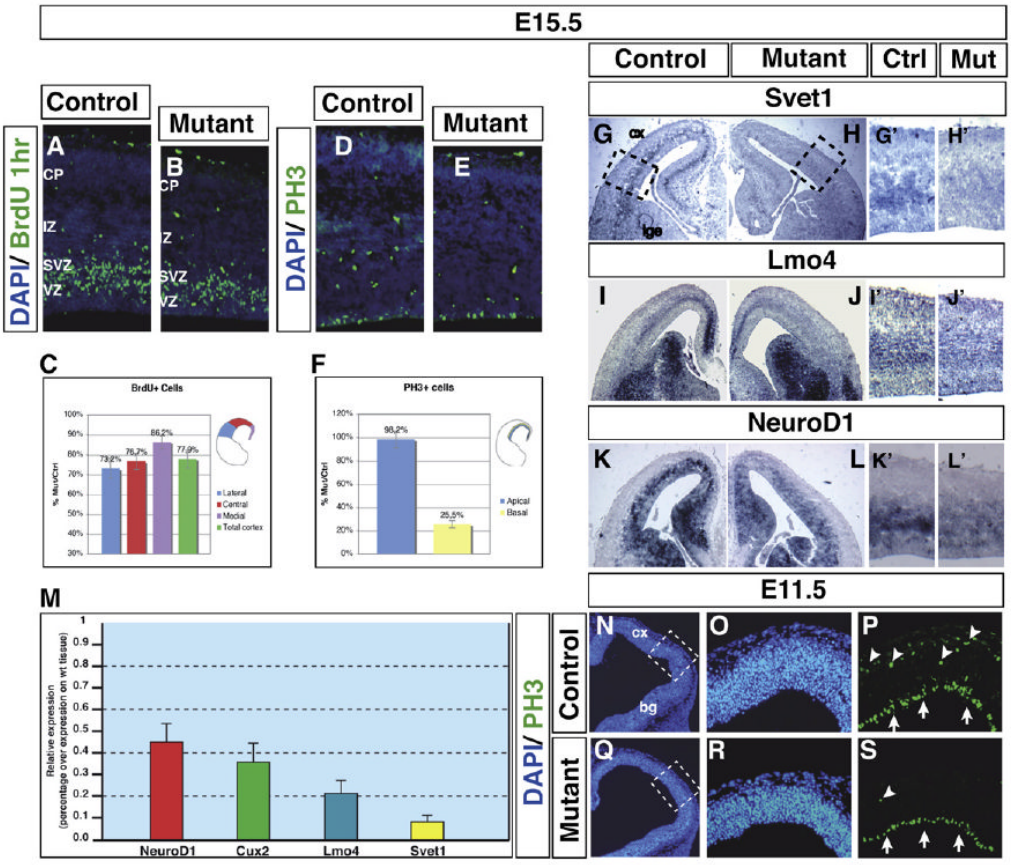

Figure 2. *Tbr2*-Deficient Cerebral Cortex Displays a Severe Loss of IPCs in the SVZ Region

(A and B) 1 hr BrdU incorporation labeling shows a reduction in S phase proliferating cells in *Tbr2* mutant with respect to control cortices. This loss is particularly evident in the basal regions corresponding roughly to the SVZ.

(C) Quantitative analysis of $BrdU^+$ nuclei reveals a 22.2% reduction shown as a ratio between mutant versus control positive cells (±3%, $p < 0.01$); with, in particular, a higher reduction in lateral (26.8% ± 5%) and central (0.77 ± 0.041) than in medial cortical fields (23.3% ± 3%).

(D and E) Strong reduction of $PH3^+$ cells in M phase residing in the SVZ region.

(F) Quantitative analysis of $PH3^+$ cells shows virtually the same number of apical (abventricular) mitoses while the basal (subventricular) ones are extremely reduced in mutant with respect to control cortices (74.5% ± 3%).

(G–L) Gene expression analysis in coronal sections of E15.5 control and *Tbr2* mutant forebrains. SVZ specific molecular markers like *Svet1* (G–H′) and *Lmo4* (I–J′) are strikingly repressed in *Tbr2*-deficient cortices, while *NeuroD1*, labeling both IPCs and their early differentiated progenies, is downregulated (K–L′). (G′), (H′), (I′), (J′), (K′), and (L′) are high-magnification views of (G), (H), (I), (J), (K), and (L), respectively.

(M) Quantitative RT-PCR analysis of the relative reduction in gene expression of the IPC molecular markers *NeuroD1* (red bar), *Cux2* (green bar), *Lmo4* (blue bar), and *Svet1* (yellow bar) in mutants with respect to controls. Results are expressed as a ratio between relative expression in WT (=1) and mutant cortices. Error bars show SD.

(N–S) Analysis of $PH3^+$ mitoses in E11.5 control (N–P) and mutant (Q–S) cortices. Basal PH3-immunoreactive dividing cells are severely reduced (arrowhead in [S]), while surface mitoses are not affected (arrows in [S]) in the mutant tissue. (N), (O), (Q), and (R) are DAPI-stained

cortical tissues and (O) and (R) are higher-power magnifications of the boxed area in (N) and (Q), respectively. bg, basal ganglia; cx, cerebral cortex; lge, lateral ganglionic eminences.

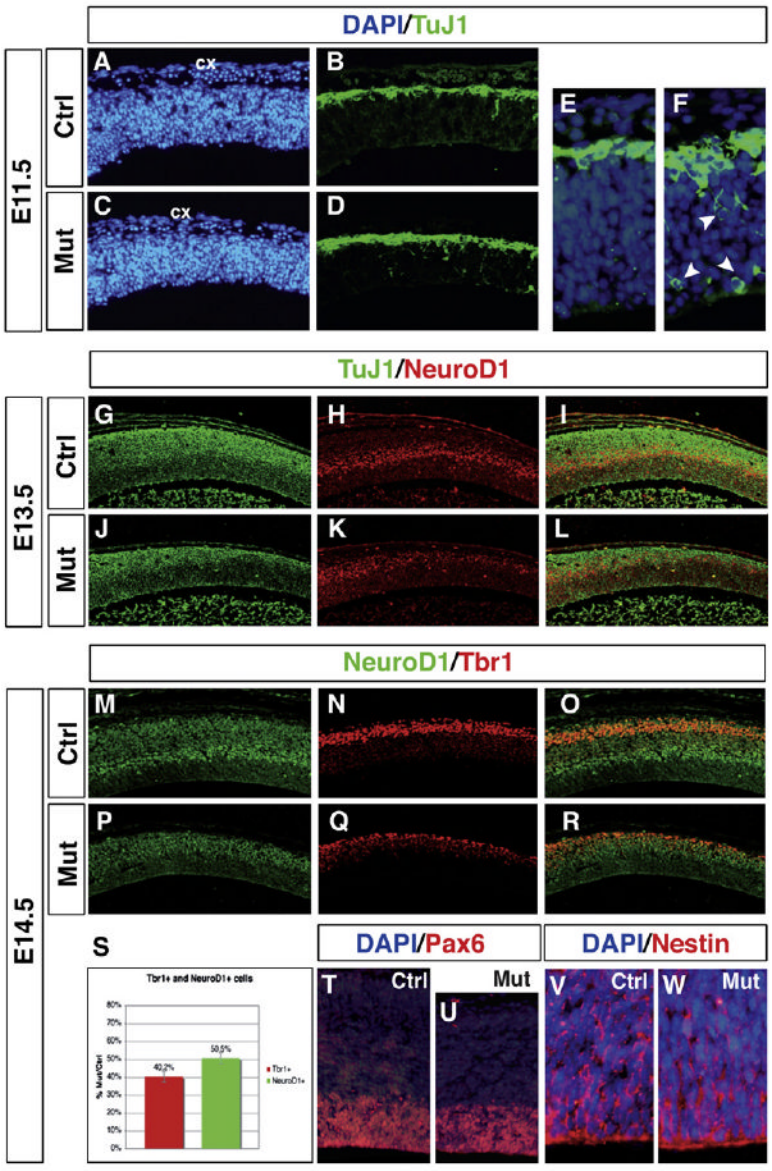

Figure 3. Loss of Tbr2 Causes an Excess of Early Neurogenesis Coupled to a Successive Reduction in Neuronal Production in Tbr2

(A–F) Immunohistochemistry for β-III-tubulin (TuJ1) on E11.5 WT (A, B, and E) and mutant (C, D, and F) cortices reveals an excessive neuronal production leading to the formation of a thicker cortical plate in the *Tbr2* mutants. Note in (F) several β-III-tubulin^{+} neurons located in the mutant VZ (arrowheads), hardly visible in the WT counterpart at this stage (E), indicating an exuberant generation of postmitotic neurons at this stage.

(G–L) Micrographs of coronal sections of E13.5 control and *Tbr2* mutant cortices immunostained for β-III-tubulin (TUJ1) and NeuroD1 reveal a notable reduction in the differentiated cortical plate tissue.

(M–R) Micrographs of coronal sections of E14.5 control and *Tbr2* mutant cortices labeled with NeuroD1 (green) and Tbr1 (red) antibody confirm a general reduction in differentiating neurons and mature early-born neurons, respectively.

(S) Quantitative analysis reveals a 59.8% ± 4% and 49.5% ± 3% reduction shown as a ratio between mutant versus control Tbr1^{+} and NeuroD1^{+} nuclei, respectively.

(T and U) Pax6-immunoreactive radial glial cells are not apparently affected in numbers and cell state by *Tbr2* ablation in E14.5 VZ.
(V and W) Morphology, organization, and general polarity of radial glial cells are not apparently affected in *Tbr2* mutant VZ as revealed by Nestin immunoreactivity. cx, cerebral cortex.

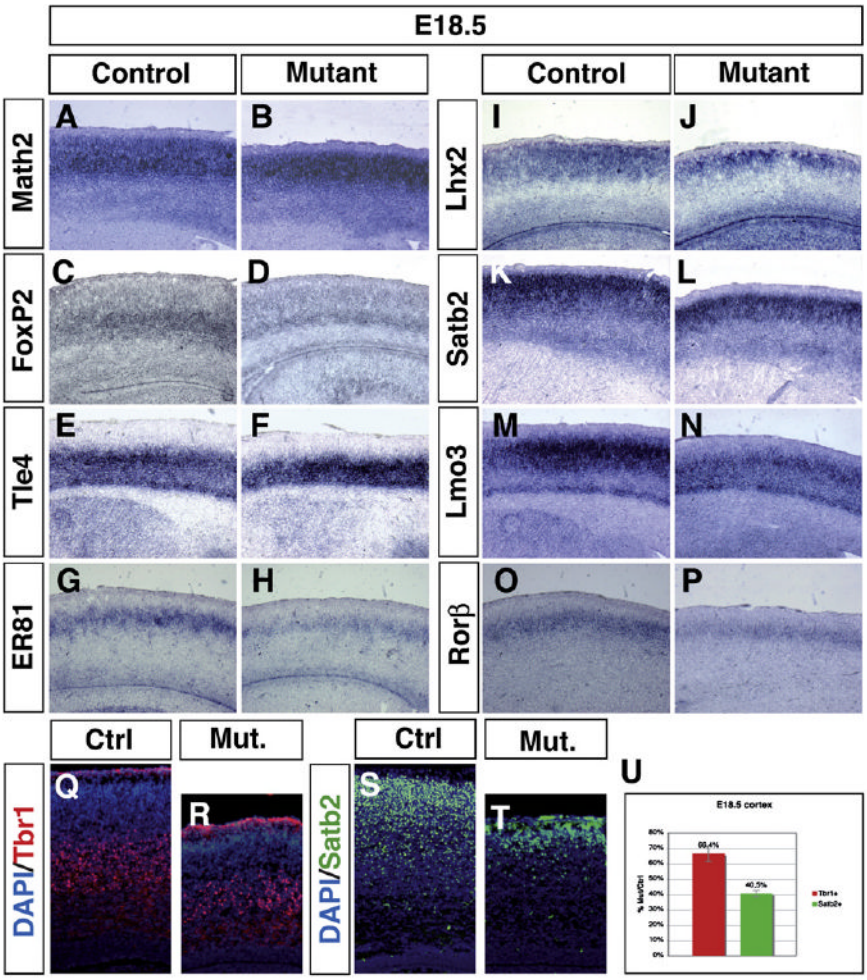

Figure 4. General Size Reduction of Cortical Layers in E18.5 *Tbr2* Mutant

(A–P) Gene expression analysis for molecular markers identifying both deeper and upper cortical layers in E18.5 control and *Tbr2* mutant forebrains. (A and B) *Math2* expression, labeling all cortical neurons, confirms a reduction of the cortical differentiated field in the *Tbr2* mutants with respect to controls.

(C–H) The expression domains of the deep cortical layer markers *FoxP2* (layerVI and subplate) (B and D), *Tle4* (layers V and VI) (E and F), and *ER81* (layer V) (G and H) are all found reduced in *Tbr2* mutant with respect to control cortices.

(I–P) The transcriptional domains of molecular markers of the superficial layer markers like *Lhx2* (layers II-III) (I and J), *Satb2* (II to IV, weak in V) (K and L), *Lmo3* (marker of layers II, III, and VI) (M and N), and *Rorβ* (layer IV) (O and P) are strongly reduced in *Tbr2* mutant with respect to control cortices.

(Q–U) Immunofluorescence staining for Tbr1 (Q and R) and Satb2 (S and T) allowed to precisely quantify the reduction of deep cortical neurons and upper cortical neurons in *Tbr2*-deficient cortices with respect to control cortices in 66.4% ± 4.5% ($p < 0.05$) and 40.5% ± 2.4% ($p < 0.05$) shown as a ratio between mutant versus control positive cells, respectively (U).

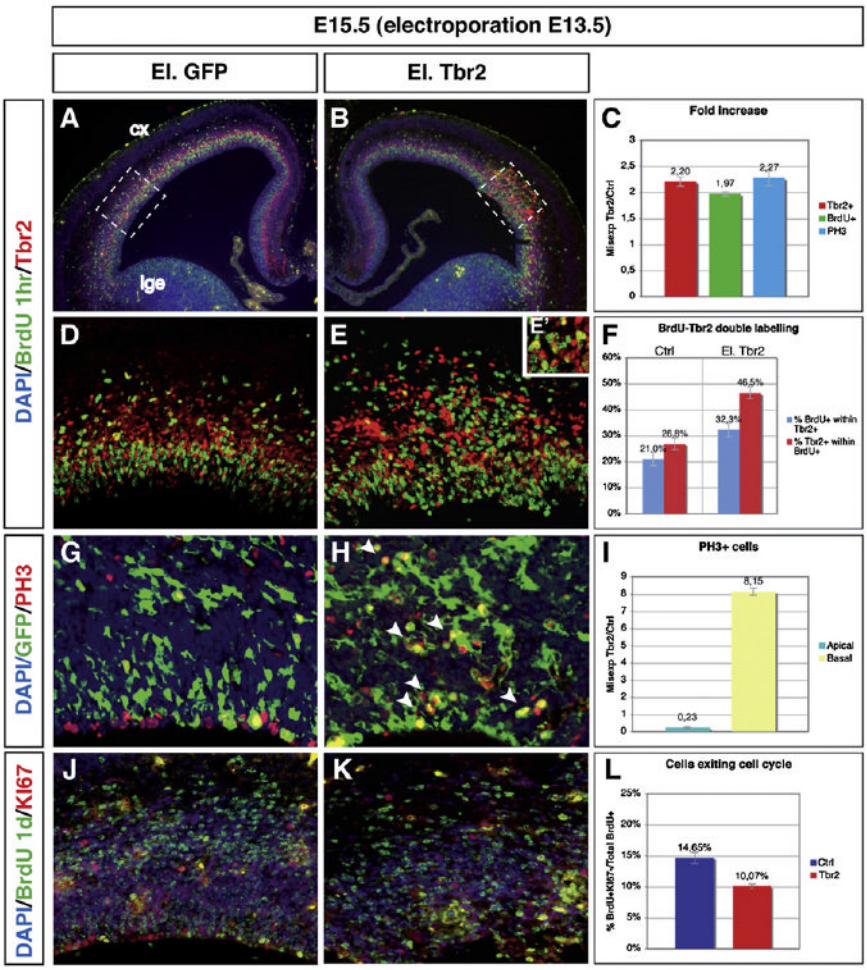

Figure 5. Misexpression of *Tbr2* Promotes SVZ Ectopic Proliferation and Cell-Cycle Maintenance

(A, B, D, and E) Distribution of S phase proliferating cells after 1 hr BrdU incorporation (green) and $Tbr2^+$ IPCs (red) in wild-type and *Tbr2* misexpressed tissue. Note the striking expansion of $BrdU^+$ cells corresponding to the basal regions between VZ and IZ. (E′) High-power view of the electroporated domain showing the close overlapping between *Tbr2* misexpressing and BrdU-positive cells.

(C) *Tbr2* misexpressing tissue displays a rough 2-fold enrichment of $BrdU^+$ cells compared to normal tissue.

(F) An increase in $Tbr2^+$ cells displaying BrdU incorporation is found in the *Tbr2* misexpressing with respect to control tissues (from 46% to 27%, respectively).

(G–I) 8-fold increase in $PH3^+$ mitotic figures in the basal regions of the neuroepithelium in Tbr2 electroporated with respect to control tissues. Note that the majority of supernumerary basal $PH3^+$ cells coexpress the EGFP reporter (arrowheads in [H]). Conversely, *Tbr2*-overexpressing cortical areas display a severe reduction of $PH3^+$ apical cells (up to 4-fold reduction).

(J–L) Double antibody staining for Ki67 (red), a marker of cells in active cell cycle, and BrdU (green) after 24 hr BrdU administration in E15.5 control and *Tbr2*-electroporated cortical areas. The fraction of $BrdU^+/Ki67^-$ cells represents the amount of cells exited from cell cycle in that specific time window. *Tbr2* misexpression promotes a reduction of $BrdU^+/Ki67^-$ labeled cells, indicating that *Tbr2* promotes proliferation and inhibits cell-cycle exit (from 14.65% to 10.07%, respectively; $p < 0.05$). cx, cerebral cortex; lge, lateral ganglionic eminence.

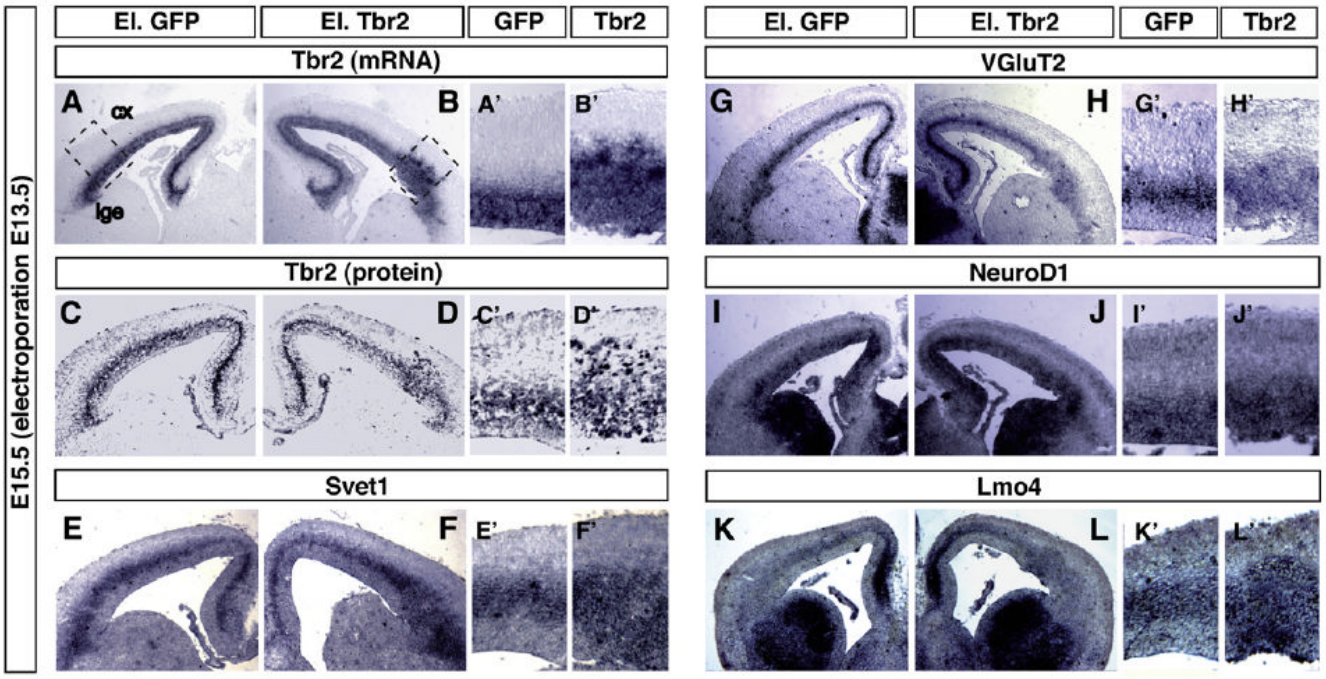

Figure 6. ***Tbr2*** **Is Sufficient to Establish SVZ-Specific Molecular Features**

(A–L′) Gene expression analysis of IPC molecular markers in coronal sections of E15.5 control and *Tbr2* electroporated cortices. *Tbr2* transcript (A–B′) and protein (C–D′) are largely expanded in *Tbr2* compared to GFP (control) electroporated cortical areas. Expression domains of SVZ molecular markers such as *Svet1* (E–F′), *VgluT2* (G–H′), *NeuroD1* (I–J′), and *Lmo4* (K–L′) are found strongly enlarged and spread both in the apical region of the VZ and in the IZ in *Tbr2*-electroporated neural tissue. (A′), (B′), (C′), (D′), (E′), (F′), (G′), (H′), (I′), (J′), (K′), and (L′) are high-magnification images of the boxed areas in (A), (B), (C), (D), (E), (F), (G), (H), (I), (J), (K), and (L), respectively. cx, cerebral cortex; lge, lateral ganglionic eminence.

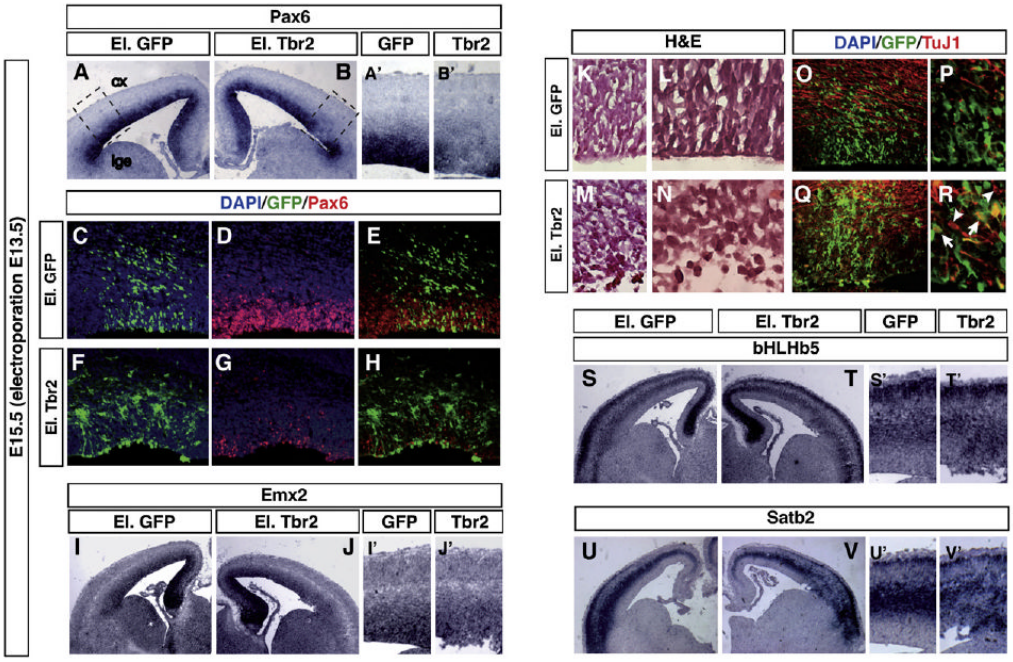

Figure 7. *Tbr2* Causes Loss of Radial Glial Cells and Their Premature Differentiation

(A–B′) In situ hybridization and immunohistochemistry (C–H) for Pax6 reveals a dramatic reduction of radial glia cells in the VZ of *Tbr2*-electroporated neural tissue, while EGFP overexpression does not exert any effect.

(G and H) $Tbr2^+$ and $Pax6^+$ cell populations remain largely separated even after *Tbr2* misexpression.

(I–J′) *Emx2*, a further marker for radial glial cells, is found similarly downregulated in the *Tbr2*-electroporated area.

(K–N) Hematoxylin and Eosin (H&E) staining of the ventricular wall of the cerebral cortex electroporated with GFP (K and L) or *Tbr2*iresGFP (M and N) expressing plasmids. While Tbr2 misexpressing tissue results is highly disorganized with deranged cells, control tissue displayed highly polarized and regular columnar cell structures.

(O–R) Immunohistochemistry for β-III-tubulin (TuJ1) (red) and EGFP (green) reveals ectopic neuronal differentiation within the VZ upon *Tbr2*, but not EGFP, forced expression. Note in (R) the presence of both β-III-tubulin$^+$/GFP$^+$ (arrows) and β-III-tubulin$^+$/GFP$^-$ cells (arrowheads) in the VZ targeted for *Tbr2* forced expression.

(S-V′) *bHLHb5* and *Sabt2* gene expression in control and Tbr2 misexpressed neural tissue. Both genes labeling postmitotic cortical cells are found ectopically expressed in the VZ upon *Tbr2*, but not EGFP, gene electroporation.

(A′), (B′), (I′), (J′), (S′), (T′), (U′), and (V′) are high-power views of boxed areas in (A), (B), (I), (J), (S), (T), (U), and (V), respectively.

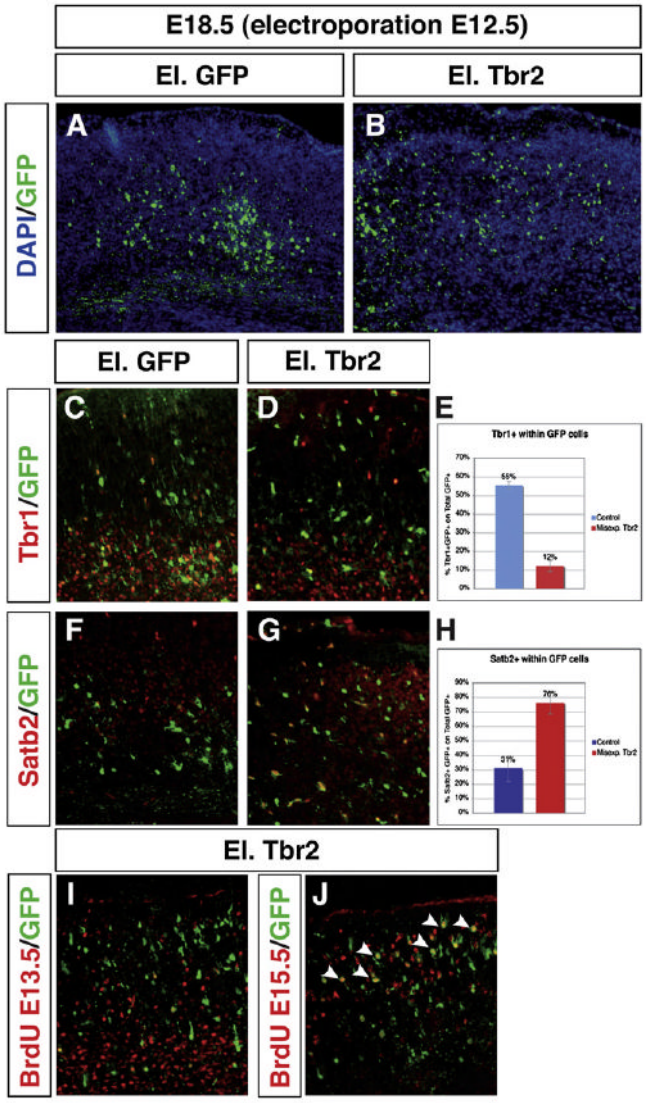

Figure 8. Long-Term Cell Fate Analysis of *Tbr2* Exogenously Expressing Cells

(A and B) Coronal sections of E18.5 cortical differentiated areas electroporated at E12.5 with plasmids expressing GFP alone or in combination with *Tbr2*. Note that GFP control cells are accumulated in the deep cortical layers while, on the contrary, a large amount of *Tbr2*-electroporated cells are found in more superficial positions.

(C–E) Photomicrographs of neocortical sections immunostained for Tbr1 and GFP show a strong reduction (up to 5-fold) in *Tbr2*-electroporated cells expressing this deep cortical key determinant with respect to EGFP-expressing cells.

(F–H) Photomicrographs of neocortical sections immunostained for Satb2 and GFP reveal a 2.5 times increase in colocalization between the two proteins in *Tbr2*-expressing cells with respect to cells expressing the EGFP only.

(I and J) High-power view of cortical tissue on coronal sections showing GFP and BrdU double labeling in E18.5 embryos subjected to E13.5 (I) or E15.5 (J) BrdU administration. Note that numerous $GFP^+/BrdU^+$ cells are found when BrdU is injected at E15.5 ([J], arrowheads), but not at E13.5 (I).